First-principles study of an $S = 1$ quasi one-dimensional quantum molecular magnetic material

Maher Yazback, Jie-Xiang Yu, Shuanglong Liu, Long Zhang, Neil S. Sullivan, and Hai-Ping Cheng*
Department of Physics, University of Florida, Gainesville, Florida 32611, USA

(Received 21 December 2019; revised 21 October 2020; accepted 5 January 2021; published 23 February 2021)

We use density functional theory to study the structural, magnetic, and electronic structures of the organometallic quantum magnet $NiCl_2$-4SC$(NH_2)_2$ (DTN). Recent work has demonstrated the quasi one-dimensional nature of the molecular crystal and studied its quantum phase transitions at low temperatures. The system includes a magnetoelectric (ME) coupling and, when doped with Br, the presence of an exotic Bose-glass state. Using the generalized gradient approximation with inclusion of a van der Waals term to account for weak intermolecular forces and by introducing a Hubbard U term to the total energy, we systematically show that our calculations reproduce the magnetic anisotropy, the intermolecular exchange coupling strength, and the magnetoelectric effect in DTN, which have been observed in previous experiments. Further analysis of the electronic structure gives insight into the underlying magnetic interactions, including what mechanisms may be causing the ME effect. Using this computationally efficient model, we predict what effect applying an electric field might have on the magnetic properties of this quantum magnet.

DOI: 10.1103/PhysRevB.103.054434

I. INTRODUCTION

Interest in materials that exhibit sizable magnetoelectric (ME) effects has grown considerably within the past decade. New classes of materials exhibiting the phenomena hint at applications where it can be harnessed, and materials can be designed for use in potential low-power spintronic devices [1] and future computing applications. The ME effect is characterized by a coupling between the magnetization and the electric polarization of a material, that is, the application of a magnetic field induces a change in the electric polarization of a material and similarly, the application of an electric field causes a change in the magnetization. Investigations into the ME effect have largely focused on its presence within transition-metal oxides [2]. Recent studies have shown that this coupling between the electric and the magnetic properties may also be present within the class of materials known as organometallic molecular crystals [2].

The fundamental building block of these solids is a molecule where individual molecular units are held together by relatively weak intermolecular interactions. At the center of each molecule is a magnetic metal ion, and the interactions between neighboring magnetic moments dictate the magnetic properties of the crystal. Given the weak interactions between molecules, molecular crystals are often easily strained under external magnetic and electric forces [3]. This soft lattice structure may provide a degree of freedom through which the ME effect may be tuned. The potential to synthesize organic ligands may also allow future flexibility in designing and tuning properties of such materials [4].

The subject of this paper is the organic quantum magnetic system dichlorotetrakisthiourea nickel, $NiCl_2$-4SC$(NH_2)_2$ (DTN) [5], which has been studied in experiments and by quantum Monte Carlo simulations based on model Hamiltonians [2,3,6–10]. The molecular unit of this system (Fig. 1) has a central magnetic Ni cation surrounded by four electrically polar ligands, $C(NH_2)_2S$ (thiourea). DTN and its doped derivatives have been studied extensively due to the rich physics present at low temperatures. The phase diagram [2,3,7] of pure DTN shows that, at temperatures below 1.2 K and below a critical magnetic-field H_{c1}, it is a quantum paramagnet. As the magnetic field, applied perpendicular to DTN's ab plane, reaches the first critical field, it experiences a quantum phase transition into an XY-antiferromagnetic (XY-AFM) state where all spins now lie within the ab plane. As the field is increased further the spins begin to cant with a corresponding increase in magnetization. When a second critical field H_{c2} is reached, the magnetization saturates and the material enters a spin-polarized state where all spins are pointing along the c axis and parallel to the applied magnetic field. Within this XY-AFM region DTN exhibits the ME effect where, along with an increase in magnetization, there is a correlated increase in the electric polarization. In this paper we investigate the structural, electronic, and magnetic properties of DTN from first principles. Using appropriate levels of approximation within density functional theory (DFT) [11,12], we are able to balance accurate structural predictions with computational efficiency to gain insight into DTN's electronic and magnetic structure, the possible mechanisms responsible for its ME effect and investigate properties of the solid.

The rest of the paper is organized as follows. Section II A presents an overview of the computational details involved in the calculations. Section II B discusses the theory behind modeling dispersion interactions and the approximations we made in attempting to obtain accurate structural properties. In Sec II C we discuss the addition of U_{eff} and the justification for our choice. In Sec. III we discuss our results relating to the

*hping@ufl.edu

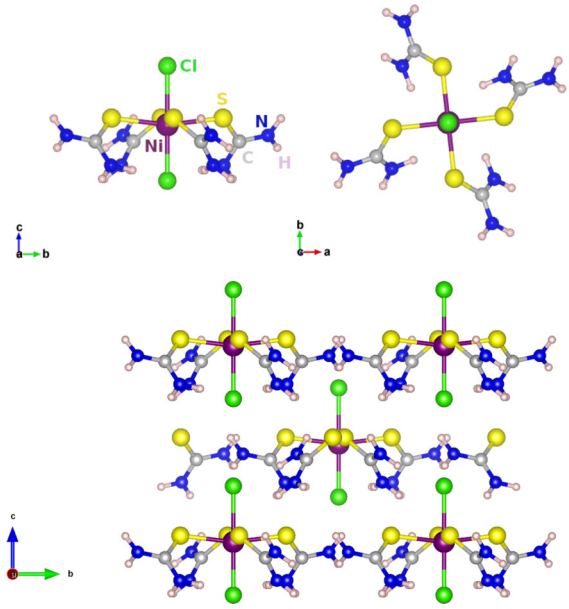

FIG. 1. (Top) Two views of the the molecular unit making up the DTN molecular crystal. Four thiourea ligands surround the magnetic Ni ion. (Bottom) The DTN unit cell.

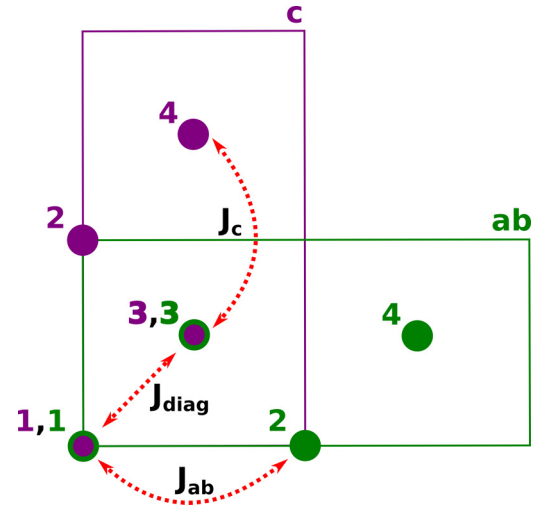

FIG. 2. The $2 \times 1 \times 1$ (*ab*, green) and $1 \times 1 \times 2$ (*c*, purple) supercells used to calculate respective exchange-coupling J values. The nodes correspond to Ni ions, and red arrows indicate the exchange interactions.

systematic improvements made to our model, comparing to experiments along the way. Finally we go on to predict experimentally unverified properties of the material and summarize our conclusions in Sec. IV.

II. METHODOLOGY

A. General

We performed first-principles calculations using the Vienna *ab initio* simulation package (VASP) [13,14] within the DFT framework.

The projector augmented-wave pseudopotentials [15,16] and generalized gradient approximations (GGA) of Perdew *et al.* [17] were used for the exchange-correlation energy. To give an appropriate description of the on-site Coulomb interaction between Ni($3d$) electrons, we apply the plus U method [18] (GGA $+ U$) with $U_{\text{eff}} = U - J = 6.0$ eV on Ni when investigating the exchange couplings and the magnetic anisotropy of DTN. The D3 [19] dispersion correction combined with GGA (GGA-D3) and/or GGA $+ U$ (GGA-D3 $+ U$) was used to take into account van der Waals (vdW) interactions. The damping parameter for D3 was set to $S_R = 1.5$. Wave functions were expanded in plane waves, and an energy cutoff of 520 eV was used for all calculations.

The Brillouin zone of the DTN unit cell containing two Ni^{2+} ions was sampled on a $6 \times 6 \times 6$ Monkhorst-Pack [20] mesh for total energy and structure optimizing calculations with an applied Gaussian smearing of 0.01 eV. A $10 \times 10 \times 10$ Γ-centered K mesh with the tetrahedron smearing method was used for the density-of-state (DOS) and orbital-resolved projected DOS (PDOS) calculation. The structure of DTN was relaxed for both the lattice constant and the atomic positions until atomic forces on each atom were converged to within 0.01 eV/Å.

Calculations of the exchange-coupling J between magnetic Ni ions were performed by creating a supercell composed of two DTN unit cells with four Ni atoms as shown in Fig. 2. In order to compare to experiment, we focused on the J_c coupling along the c axis of the unit cell and J_{ab} coupling between Ni ions within the *ab* plane or along the a/b axis. In addition, the J_{diag} coupling, which connects the corner Ni with the body-centered Ni ion was also considered. Two supercells, one of $1 \times 1 \times 2$ extending along the c axis and the other of $2 \times 1 \times 1$ extending along the a/b axis, were created to isolate inequivalent Ni ions. The corresponding K mesh was, therefore, $6 \times 6 \times 2$ or $2 \times 6 \times 6$, respectively.

In order to gain insight into the magnetic interactions in DTN, we transformed the plane-wave-based Bloch states from VASP into Wannier function- (WF-) based local states by using the maximally localized Wannier functions method [21] implemented in the WANNIER90 package [22]. By choosing an initial guess of projections from the outer energy window, an effective tight-binding Hamiltonian $\mathcal{H}$ was built in a downfolded Hilbert subspace where the eigenvalues in the inner energy windows are exactly the same as those of DFT results [23]. Microscopic insights into the relevant orbitals and superexchange paths in DTN are based on the hopping integrals and on-site energies of the WF-based Hamiltonian, $\mathcal{H}$.

Magnetic anisotropy is a consequence of spin-orbit interactions; we, therefore, performed noncollinear magnetic DFT calculations including spin-orbit interactions. We obtained the total energies for various configurations with each having a set of constrained directions of the local magnetic moments for the Ni atoms. The resulting total energy difference between configurations with moments perpendicular to one another gave the magnetic anisotropic energy. The direction with the lowest total energy is usually labeled as the easy axis.

It is worthwhile mentioning that when we study effects of an electric field, VASP calculates the response of system properties to the electric field without applying an explicit external global field. This approach is based on the modern theory

TABLE I. Lattice constants of DTN with optimized structures obtained using different exchange-correlation functionals.

XC functional	a (Å)	c (Å)
GGA	9.70	9.35
GGA-D3 ($S_R = 1.2$)	9.55	8.78
GGA-D3 ($S_R = 1.5$)	9.58	8.92
DF2	9.77	9.02
optB88	9.54	8.63
Experiment [5]	9.56	9.08

of polarization [24,25] in which the electric polarization is written in terms of a Berry phase in order to circumvent the periodic boundary condition problem. The energy includes a term that is a function of polarization, a variational principle is applied with the inclusion of such term, and the total energy in the presence of an external electric field is, thus, obtained. The implementation of such a treatment is not a simple matter. A brief description can be found in the VASP online manual [26]. Further references include the paper by Souza *et al.* [27] which follows the perturbation expression after discretization approach of Nunes and Gonze [28]. One can also apply an electric field by setting dual gate configurations in which the Poisson equation is solved with given boundary conditions to obtain the unique solution for the electrostatic potential. A review of this subject can be found in our recent article [29].

B. Test of the van der Waals correction

Molecular crystals pose a challenge to the theorist when trying to predict their structural properties. This has been especially true for GGA exchange-correlation functionals in DFT calculations, which struggle to account for long-range correlations, such as the vdW force [30] and hydrogen bonding. New functionals optB88 [31] and DF2 [32] have been introduced recently to model these dispersive interactions accurately. In order to balance the computational cost of calculations while still accurately predicting molecular structures, we also consider the D3 [19] dispersion correction, which is frequently cited for successfully predicting molecular crystal structures. The D3 dispersion adjusts the internuclear energy to account for long-range asymptotic behavior with little effect at short range, giving an augmented DFT total energy.

We chose the vdW correction for our paper after performing a benchmark test for the lattice constants of DTN. The DTN unit cell with two Ni atoms was used. The collinear magnetic moments on the two magnetic Ni atoms in the unit cell are aligned antiparallel. Structures were optimized for both lattice and atomic positions. The lattice constants for the DTN molecular crystal were investigated with various functionals and were compared with experimental data. The resulting tetragonal lattice constants a and c are listed in Table I. Without any vdW correction, both lattice constants a and c are severely overestimated whereas using the GGA functional, the c lattice constant is especially, being 0.27 Å larger than the experimental value, indicating the failure to consider long-range vdW interactions with GGA. Among the three vdW corrections GGA-D3, optB88, and DF2, optB88 underestimates lattice constants, especially c with a 0.45-Å difference compared to the experimental values. DF2 has small deviations, 0.21 Å for a and 0.06 Å for c, respectively, compared to the experimental values. GGA-D3 with the default value of damping parameter $S_R = 1.217$ overestimates the vdW interaction so that it has a relatively large deviation of 0.30 Å for c, compared to the experimental value. GGA-D3 with a damping parameter $S_R = 1.5$ gives the best agreement with the experimental data. The deviation is only 0.02 Å for a and 0.16 Å for c. Considering that the D3 dispersion correction has less computational cost and performs better than optB88 and DF2, we employed GGA-D3 and GGA-D3 + U with the adjusted damping parameter for our future calculations on DTN. The lattice constants of DTN were set to $a = 9.58$ Å and $c = 8.92$ Å, the GGA-D3 result for the rest of our calculations.

C. Estimation of U_{eff}

Constrained random phase approximation (cRPA) calculations [33,34] for the Ni site were carried out using the full-potential linearized augmented plane-wave method implemented in the EXCITING-PLUS code [35] to have a reasonable estimate of the on-site Coulomb interaction of the Ni($3d$) orbitals.

The basic idea of cRPA is to calculate a partial RPA particle-hole polarization with the constraint of a physically motivated correlation window, for example, the d-like bands around the Fermi level. The on-site screened Coulomb interaction strength then can be determined from the partial RPA particle-hole polarization and the bare Coulomb interaction. The RPA polarization is obtained from Kohn-Sham susceptibility, which is completely based on the DFT ground state. We benchmarked it against other implementations using late transition-metal monoxides and got consistent results [36].

The molecular unit of DTN, as shown in Fig. 1, that was used has the Ni sitting in the center of the octahedron formed by four S atoms and two Cl atoms. A unit cell with bulk lattice constants but containing a single DTN molecule with 35 atoms in total was taken into account. This is enough for the calculation of the Kohn-Sham susceptibility and partial RPA polarization because the molecule is well separated from its nearest neighbors in the diagonal directions, and the feature of the strong interaction along the c axis is preserved. The resulting diagonal elements of the U matrix, the on-site U, of d orbitals is ∼4.9 and $J \sim 0.5$ eV. The cRPA calculation scheme is based on a paramagnetic ground state, and magnetic properties of the material are not taken into account so that the Pauli exclusion principle is not included in the calculation. This ignorance causes underestimation of the U values [36]. Thus, $U = 4.9$ eV is considered as a lower bound for the value of U_{eff} for our GGA-D3 + U calculations.

A self-consistent calculation using the $+U$ approach may possibly leave the system trapped in local a minimum. To resolve this problem, we performed occupation matrix control for the Ni atoms in the DTN system. In our calculation, we used a $U_{\text{eff}} = 6.0$ eV following the Dudarev scheme and without spin-orbit coupling as implemented in VASP [37]. Since each Ni^{2+} ion has eight d electrons, they fully occupy all five d orbitals in the spin-majority channel and three in

TABLE II. Average exchange-coupling J^{avg} in units of meV along the c axis and on the ab plane using GGA and GGA + U, compared to the experimental results.

XC	J_c^{avg}	J_{ab}^{avg}	J_{diag}
GGA-D3	−1.05	−0.149	−0.033
GGA-D3 + U (4.9)	−0.28	−0.023	−0.010
GGA-D3 + U (6.0)	−0.21	−0.018	−0.008
GGA-D3 + U (7.0)	−0.16	−0.015	−0.006
Experiment	−0.19	−0.016	Not available

the spin-minority channel. We, thus, manually set $C_5^3 = 10$ constrained occupation matrix configurations (1.0 for each occupied orbital and 0.0 for each empty one for the diagonal elements of the matrix) in the spin-minority channel. After running self-consistent calculations using constrained occupation matrices, we removed the constraint and continued the calculations. Both the ferromagnetic and the AFM spin orderings in one unit cell with two Ni atoms were employed for the test. The results show that two self-consistent solutions for the Ni ion were identified. One is the nonmagnetic solution with $S = 0$ on Ni, and the other has $S = 1$ on Ni, which is the same on-site spin state we used throughout our calculations in the paper. The nonmagnetic solution is 3 eV higher in total energy than the $S = 1$ state. The numerical difference for matrix elements with various spin ordering and/or U/U_{eff} values is within 0.02, indicating the robustness of the ground state. We, therefore, confirmed that we were able to obtain the Kohn-Sham ground state in the DTN system using the occupation matrix control method. A similar procedure is applied to a few other spin configurations to make sure we obtain the desired states.

To further understand the influence of U_{eff} on the results of our GGA-D3 + U calculations, we calculated J_c couplings along the c axis for various U_{eff} values. We used the structures obtained with the GGA-D3 functional for this benchmark test. The results are shown in Table II. The value of J_c for $U_{\text{eff}} = 4.9$ and $J = 0.52$ eV (calculated by cRPA) is −0.31 meV and for $U_{\text{eff}} = 4.9$ and $J = 0.0$ eV is −0.28 meV. The experimental value [7] is −0.19 meV (−2.2 K) where the negative value corresponds to an antiferromagnetic coupling. This is a significant improvement over the GGA-D3 value of −1.05 meV. Since $U - J$ only adds a small correction, for the rest of the test we set $J = 0.0$ eV for simplicity: Then the values of J_c for $U_{\text{eff}} = 6.0$ and 7.0 eV are −0.21 and −0.16 meV, respectively. Considering the U_{eff} values used in the previous experimentally validated bulk NiO calculations [18,38] and the results mentioned previously, we finally chose $U_{\text{eff}} = 6.0$ eV for our GGA-D3 + U calculations.

Both the Liechtenstein and Dudarev schemes with an isotropic correction of U or U_{eff}, may violate Hund's first rule and result in artificial spin angular momenta, leading to an unsatisfactory description of magnetic anisotropy energies. An anisotropic correction was suggested by Ylvisaker *et al.* [39] to resolve the problem. In the DTN system, Ni^{2+} ions have $L = 0$, $S = 1$ orbital and spin states, respectively, which are determined correctly before the spin-orbit interaction is applied. The anisotropic correction only adds a constant term in this case making the isotropic correction enough here. The U_{eff}-dependent magnetic anisotropy energies were obtained with various U_{eff} values. The energy difference between spins along the c axis and spins along the a axis is 0.78–0.79 meV (9.05–9.16 K) per unit cell for GGA-D3 + U with $U_{\text{eff}} = 4.9$–7.0 eV, showing the anisotropy is insensitive to U_{eff}. Here we set $J = 0$ eV. An effort to implement the correction of Ylvisaker *et al.* [39] is needed for future investigations. Here, we present the results from +U approach along with $U = 0$ results with the understanding of its potential drawbacks in magnetic anisotropy (MAE). For completeness we calculated the magnetic anisotropy using $U = 4.9$ and $J = 0.52$ eV in the Liechtenstein scheme, giving an anisotropy value within the 0.78–0.79-meV window, which will be discussed again in Sec. III C.

TABLE III. Bond lengths and bond angles of structurally relaxed DTN using GGA-D3 compared to experiment.

Bond length (Å)	Experiment	Calculated
Ni-Cl(1)	2.40	2.41
Ni-Cl(2)	2.52	2.54
Ni-S	2.46	2.44
S-C	1.73	1.72
C-NH_2(1)	1.34	1.34
C-NH_2(2)	1.32	1.33
Bond angle (°)		
S-Ni-Cl(1)	96.7	96.8
S-Ni-Cl(2)	83.3	83.2
Ni-S-C	113.9	114.2
S-C-NH_2(1)	116.9	119.4
S-C-NH_2(2)	122.3	121.3
NH_2(1)-C-NH_2(2)	120.8	119.2

III. RESULTS AND DISCUSSION

A. Structural properties

The Ni atoms in DTN form a body-centered tetragonal lattice so that there are two Ni atoms, one at the corner and the other at the body center, in each tetragonal unit cell of DTN. Each Ni, with a +2 valence state, is surrounded by four S atoms on the ab plane and two Cl atoms along the c direction, leaving them in an octahedral crystal field. In each NiS_4Cl_2 octahedron, Cl atoms are located exactly on the apical sites along the c axis, whereas S atoms in the polar thiourea ligands $C(NH_2)_2S$ deviate a little from the ab plane containing the central Ni.

A comparison of bond lengths and bond angles between the DFT relaxed structure using GGA-D3 and experiment [5] is given in Table III. Bond lengths are all within 0.02 Å and bond angles are within 2.5° of the experimental values. This further confirms the consistency between the GGA-D3 approach and the experiment.

B. Exchange coupling

Each magnetic Ni ion in molecular crystal DTN has spin $S = 1$. The tetragonal DTN bulk has two nonequivalent Ni-Ni spin couplings, one along the c axis and another on the

ab plane. The corresponding spin Hamiltonian in terms of Ni magnetic spins is

$$\mathcal{H}_s = -J_c \sum_{\langle i,j \rangle} S_i S_j - J_{ab} \sum_{\langle l,m \rangle} S_l S_m + D \sum_i \left(S_i^z\right)^2 - g\mu_B H \sum_i S_i^z, \quad (1)$$

where $\langle i, j \rangle$ and $\langle l, m \rangle$ are the out-of-plane and in-plane neighbors, respectively, D is the coefficient of on-site uniaxial magnetic anisotropy, also known as the zero-field splitting, and $g\mu_B H$ is the interaction with an external magnetic field.

Experimentally it has been found that the exchange-coupling J_c between Ni ions along the c axis is an order of magnitude larger than the coupling J_{ab} within the *ab* plane [7]. It is, thus, suggested that spins in DTN behave as quasi one-dimensional (1D) spin chains. Therefore, we investigated the exchange coupling using the molecular crystal structures obtained from GGA-D3. As described in the methods section, the calculations for the exchange coupling J values involved creating two supercells, shown in Fig. 2, extended along the *ab* (green) and c directions (purple) to isolate the couplings of interest. We computed DFT total energies for various inequivalent spin configurations and fit the exchange-coupling J parameters to the Heisenberg model. Table II gives the calculated results for the exchange-coupling J for GGA-D3 and GGA-D3 + U (with $U_{\text{eff}} = 6.0$ eV) compared to the experimental data. Both experiments and theory show that J_c is negative, an antiferromagnetic coupling with strength an order of magnitude larger than J_{ab}.

Compared with the experimental value of -0.190 meV (-2.2 K), J_c with GGA-D3 is severely overestimated to be -1.05 meV (-12.2 K). The calculated J_{ab} is -0.149 meV (-1.73 K) using GGA-D3, which is also an order of magnitude larger than the experimental value -0.016 meV (-0.18 K). On the other hand, the GGA-D3 + U with the adjusted U_{eff} value gives results consistent with the experimental values for both J_{ab} and J_c. Although the two Ni ions are nearest neighbors, values of J_{diag}, the coupling between a corner Ni, and a body-centered Ni are even weaker than J_{ab} for both functionals. Because of the negligible values of both J_{ab} and J_{diag}, the strong J_c coupling makes DTN a quasi-1D antiferromagnetic chain along the c axis.

Experiments suggest that strong exchange coupling along the c axis is via the Ni-Cl-Cl-Ni chain [7]. To examine the interatomic interactions, we investigated the electronic structure of the DTN unit cell with antiferromagnetic ordering. The resulting DOS is shown in Fig. 3. The total DOS in panel (a) shows that DTN is insulating with a wide band gap of about 2.5 eV. In panel (b), the Ni $d_{3z^2-r^2}$ (red) and $d_{x^2-y^2}$ (blue) orbitals, often called e_g orbitals in an octahedral crystal field, are fully occupied in the spin-majority channel, and those in the spin-minority channel are almost fully empty, indicating a $S = 1$ spin state of the Ni^{2+} cation. In panels (d) and (e), Cl-Cl bonding and antibonding states are identified. The cross sections of the partial charge densities for these states are shown in panel (f). In the bonding state, an overlap between the two Cl($3p$) ions appears, whereas there is a node between the two

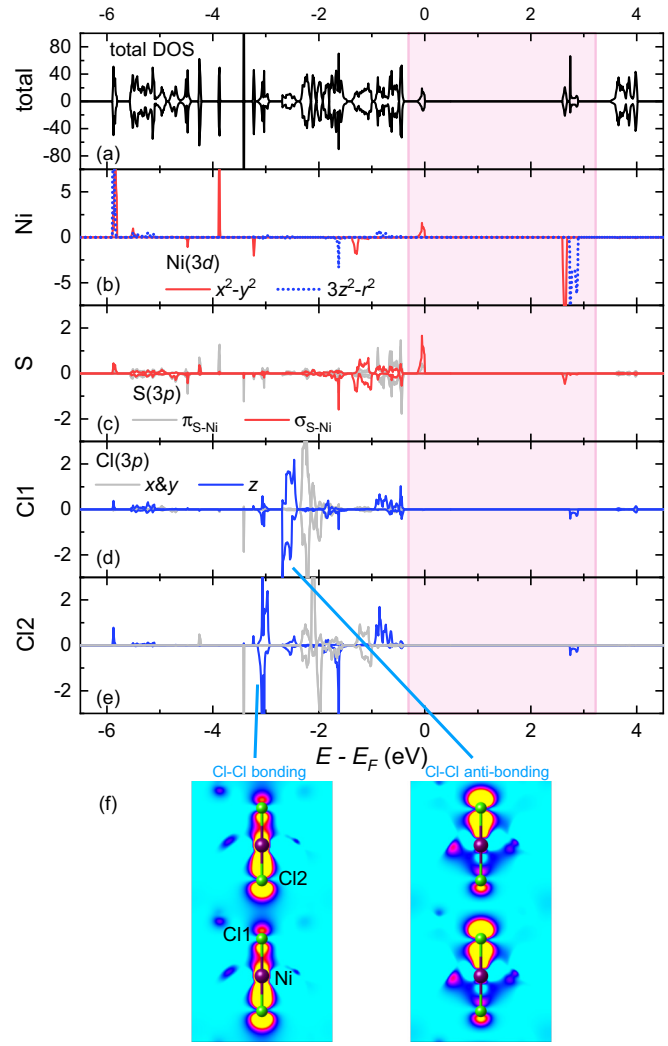

FIG. 3. DOS of the DTN unit cell using the GGA-D3 + U approximation. Panel (a) is the total DOS. Panels (b)–(e) are orbital-resolved PDOS. Panel (b) shows $d_{3z^2-r^2}$ (red) and $d_{x^2-y^2}$ (blue) (e_g) orbitals of Ni($3d$); (c) S $3p$ orbitals forming S-Ni σ bonds and π bonds, respectively; and (d) and (e) Cl($3p$) orbitals of Cl1 and Cl2 identified in (f). Positive and negative values correspond to spin-majority and spin-minority channel, respectively. The Fermi level is set to zero. The shaded region is the inner energy window for constructing the Wannier-based tight-binding Hamiltonian. The cross section in a $1 \times 1 \times 2$ supercell in (f) shows the partial charge densities of Cl-Cl bonding and antibonding states labeled in (d) and (e).

Cl ions in the antibonding state. The splitting between them is about 0.4 eV. The Cl-Cl distance is about 4.0 Å, much larger than the Cl-Cl bond length in Cl_2, and the energy splitting is smaller than a typical $pp\sigma$ bond but is still much larger than the energy of the van der Waals interaction. Therefore, it reflects strong intermolecular interactions through the Cl-Cl chain along the c axis. We note that Cl($3p$) orbitals hybridize with the Ni($d_{3z^2-r^2}$) orbitals at about 0.5 eV below the Fermi level in the spin-up channel and about 3 eV above the Fermi level in the spin-down channel [Figs. 3(b), 3(d), and 3(e)]. On the plane of NiS_4 in the NiS_4Cl_2 octahedron, S atoms along S-Ni-S and along the a and b axes are labeled as S_x and S_y,

respectively. In this case, $S_x(p_x)$ and $S_y(p_y)$ form σ bonds with $Ni(d_{x^2-y^2})$ so that they are labeled as $S(\sigma_{S\text{-}Ni})$ in panel (c). Just below the Fermi level, $Ni(d_{x^2-y^2})$ hybridizes with $S(\sigma_{S\text{-}Ni})$.

To understand the hybridization and the magnetic interaction pathway, we performed a unitary transformation on Bloch states to construct Wannier orbitals and the tight-binding Hamiltonian. We used a $1 \times 1 \times 2$ supercell with antiferromagnetic coupling along the c axis and $Ni(e_g)$ orbitals on each Ni ion were used as initial projections. In this case, a total of eight Wannier functions for each spin channel are localized exclusively on Ni ions. The inner energy window we chose from -0.25 to 3.2 eV is shown in Fig. 3. It covers both the valence and the conduction bands and so captures features of the gap for the virtual excitation in the exchange picture. The outer energy window covers all occupied states and the unoccupied states below 0.5 eV. The isosurface in Fig. 4 shows one of the Wannier orbitals, which has features of $Cl(p_z)$, $S(\sigma_{S-Ni})$, and $Ni(e_g)$. These characteristics signal strong hybridization. The corresponding matrix elements, in units of eV, including nearest-neighbor hopping t and the on-site energy ε in the WF basis, are

$\mathcal{H}_{mn}$ (eV)	$\lvert 1^o_{3z^2-r^2}\rangle$	$\lvert 1^o_{x^2-y^2}\rangle$	$\lvert 2^u_{3z^2-r^2}\rangle$	$\lvert 2^u_{x^2-y^2}\rangle$	$\lvert 3^o_{3z^2-r^2}\rangle$	$\lvert 3^o_{x^2-y^2}\rangle$	$\lvert 4^u_{3z^2-r^2}\rangle$	$\lvert 4^u_{x^2-y^2}\rangle$
$\langle 1^o_{3z^2-r^2}\rvert$	−5.540	0.000	**−0.031**	0.000	0.000	0.023	0.000	0.000
$\langle 1^o_{x^2-y^2}\rvert$		−0.287	0.000	0.001	0.002	0.004	0.001	0.000
$\langle 2^u_{3z^2-r^2}\rvert$			2.570	0.000	0.005	−0.006	0.005	−0.008
$\langle 2^u_{x^2-y^2}\rvert$				2.405	−0.008	−0.002	−0.004	0.000
$\langle 3^o_{3z^2-r^2}\rvert$					−5.547	0.000	**−0.031**	0.000
$\langle 3^o_{x^2-y^2}\rvert$						−0.287	0.000	0.001
$\langle 4^u_{3z^2-r^2}\rvert$		H.c.					2.570	0.000
$\langle 4^u_{x^2-y^2}\rvert$								2.405

(2)

The position labels 1 to 4 of the WFs are the same as those in Fig. 2. The subscripts $3z^2 - r^2$ and $x^2 - y^2$ represent the $3z^2 - r^2$-like and $x^2 - y^2$-like WFs centered on each Ni. Superscripts o and u refer to WFs with negative and positive on-site energies, respectively.

In particular, the largest hopping t between occupied and unoccupied WFs is -0.031 eV [indicated in bold in Eq. (2)], which comes from two $3z^2 - r^2$-like WFs of neighboring unit cells along the c axis. Considering the difference in on-site energies Δ of associated WFs on Ni ions along the c axis, we can estimate the magnitude of their exchange interaction by $J_c \sim 4t^2/\Delta$ to be about 0.474 meV (5.5 K). Other hopping elements between WFs centered on Ni ions with distinct occupied states are much smaller (around -0.001 eV or less), indicating a smaller exchange interaction along the diagonal direction and the a/b-axis directions. Overall, our results show that, although our estimate is of the right order of magnitude using a tight-binding model in the Wannier basis, using energetics and fitting to a Heisenberg model provides better J-coupling values compared to experiment. An alternative WF-based Hamiltonian using atomic-centered projection (see the Supplemental Material for details [40]) further confirms the strong hopping between intermolecular $Cl(p_z)$-$Cl(p_z)$ orbitals that plays a key role in the superexchange interaction. What we gain from our Wannier analysis [41] is more insight into the orbital contributions to the superexchange pathway.

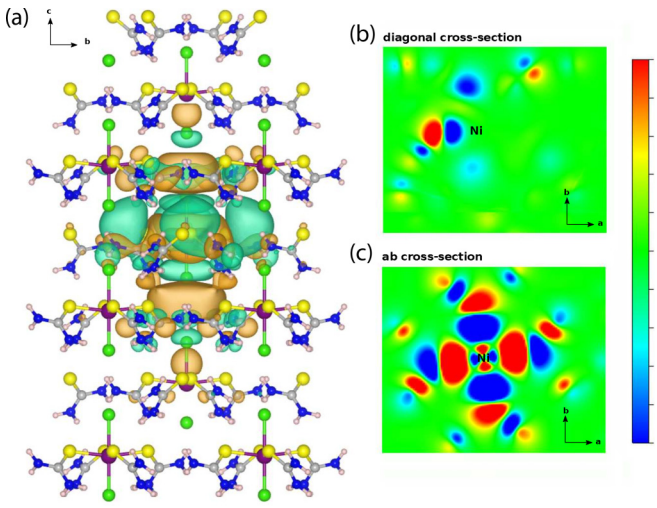

FIG. 4. (a) Isosurface of a Wannier function for the AFM c-axis supercell, indicating hybridization of Ni and Cl orbitals leading to a superexchange path along the Ni-Cl-Cl-Ni chain; (b) Wannier orbital in a cross section containing two Ni ions along a diagonal line of the lattice; and (c) on the ab plane of the lattice.

C. Magnetic anisotropy

Besides the exchange coupling J, another important interaction in Eq. (1) is the magnetic anisotropy. To study the magnetic anisotropy in DTN, we performed spin-constrained DFT calculations including the spin-orbit interaction and noncollinear magnetic moments for both an isolated DTN molecule and a DTN molecular crystal. We first look at the isolated molecule, which is placed in a $20 \times 20 \times 20$-Å supercell with adequate vacuum space, and only the Γ point in reciprocal space is calculated. The functional used in calculations is GGA-D3. By setting a series of constrained directions of the Ni spin, the total energies $E(\theta, \phi)$ as a function of direction angles are obtained. In the crystal unit cell with two Ni atoms, the corner Ni spin is fixed to be aligned along the c axis, and a different spin direction for the body-centered Ni is sampled using spherical coordinates. The resulting relative

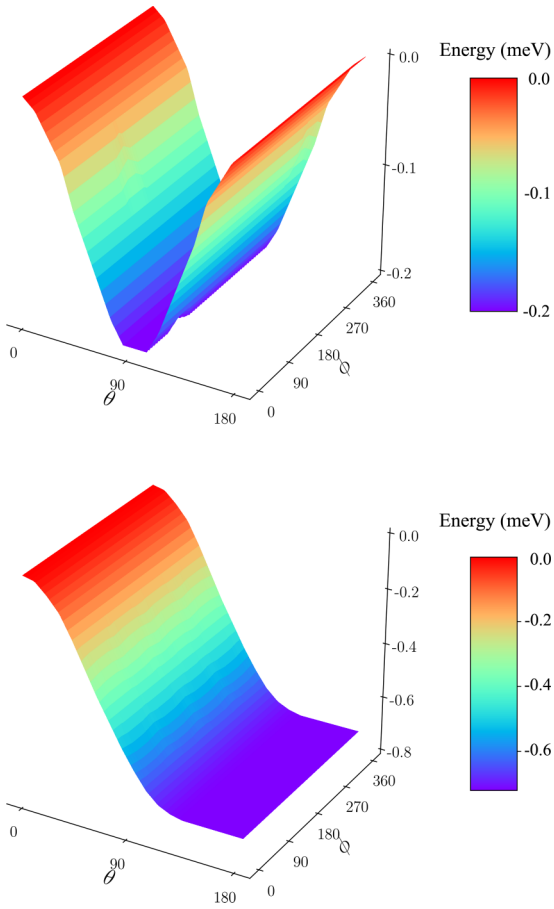

FIG. 5. Relative total energy as a function of the angle between the c axis and the spin of the Ni ion for (top) the DTN molecule and (bottom) the DTN unit cell with the other inequivalent Ni ion spin fixed along the c axis. The angles θ and ϕ refer to the orientation angles in spherical coordinates.

energy maps for $E(\theta, \phi)$ are shown in Fig. 5. In the case of a single DTN molecule, the lowest energy is at $\theta = 90°$, the in-plane direction, and the highest energies are at $\theta = 0°$ and 180° when the spins are along the c axis. Since the energy as a function of ϕ is almost invariant, this indicates that the ab plane is the easy axis with little ϕ dependence, and the c axis is the hard axis. The energy difference $E(0°, \phi) - E(90°, \phi)$ is 0.20 meV (2.3.2 K). This result shows a uniaxial magnetic anisotropy of the DTN molecule. For the molecular crystal, $E(0°, \phi)$ is the highest whereas $E(180°, \phi)$ is the lowest. The energy difference $E(0°, \phi) - E(180°, \phi)$ is 0.59 meV (6.84 K). Since the spin of the corner Ni is fixed along the c axis, the direction of the central Ni spin with lowest energy corresponds to antiferromagnetic spin ordering with the corner Ni spin.

The definition of D, the zero-field splitting, is the energy difference between states with $|S_z = \pm 1\rangle$ and $|S_z = 0\rangle$ for a $S = 1$ system. DFT calculations can only give the quantum state,

$$|S_x = \pm 1\rangle = \frac{1}{2}|S_z = 1\rangle \pm \frac{1}{\sqrt{2}}|S_z = 0\rangle + \frac{1}{2}|S_z = -1\rangle \quad (3)$$

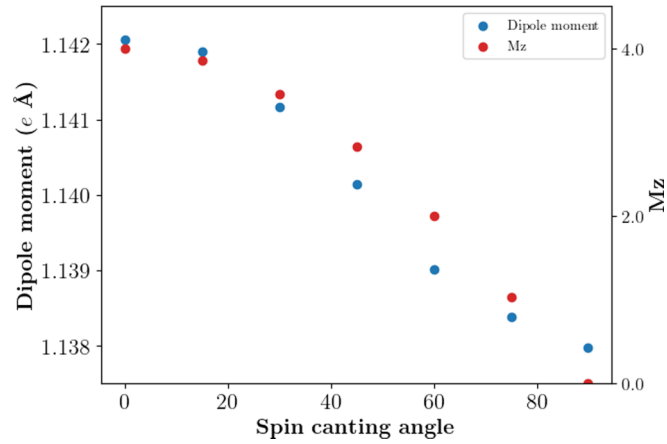

FIG. 6. Magnetoelectric coupling in DTN. The electric dipole moment (blue) and the z component of the magnetization (red) are plotted as a function of the spin canting angle of the spin moment on the Ni cation.

instead of $S_z = 0$ when the spin is constrained along the a axis. To calculate the magnetic anisotropy for the unit cell with two Ni atoms, we take the energy difference between configurations where the spins in one configuration are aligned along the c axis and along the a axis for the other configuration. The energy difference $E(0°, \phi) - E(90°, \phi)$ per Ni by DFT is $D[1^2 - [\frac{1}{4}1^2 + \frac{1}{4}(-1)^2 + \frac{1}{2}0^2]] = \frac{1}{2}D$. Therefore, $D = 2[E(0°, \phi) - E(90°, \phi)]$ for DTN. The experimental value is $D = 0.774$ meV (8.98 K).

For the DTN crystal, we performed both GGA-D3 and GGA-D3 + U with $U_{\text{eff}} = 6.0$ eV. Using the GGA-D3 functional, we underestimate D to be 0.54 meV (6.26 K). A GGA-D3 + U calculation gives $D = 0.78$ meV (9.10 K), consistent with the experimental results. We also examined $U = 7.0$ eV and $U - J$ with $U = 4.9$ and $J = 0.52$ eV calculated by cRPA and found that D is insensitive corresponding to a D value of 0.78 meV for both. It is worth noting that for heavy elements that involve f electrons, a nonspherical $U - J$ scheme may be needed [42].

A fuller investigation of magnetic anisotropy, including the effects of substitutions of Cl ions and ligands, will be left for future work. Earlier results suggest a decrease in magnetic anisotropy as the substitute ion gets larger [43].

D. Magnetoelectric effect

With an understanding of the magnetic interactions in DTN we turn to the ME effect. To investigate this effect we again performed spin-constrained DFT calculations, including the spin-orbit interaction and noncollinear magnetic moments. This was performed for the DTN molecular crystal with two Ni atoms and using the GGA-D3 functional and its corresponding relaxed structure. Constraining the moment direction of each Ni relative to the c axis allowed us to simulate what magnetic configurations would result when a magnetic field is applied parallel to the c axis of the molecular crystal. The spin canting angle in Fig. 6 is equivalent to the polar angle relative to the c axis. A spin-canting angle of 0° corresponds to spins that are parallel to the c axis and representing the

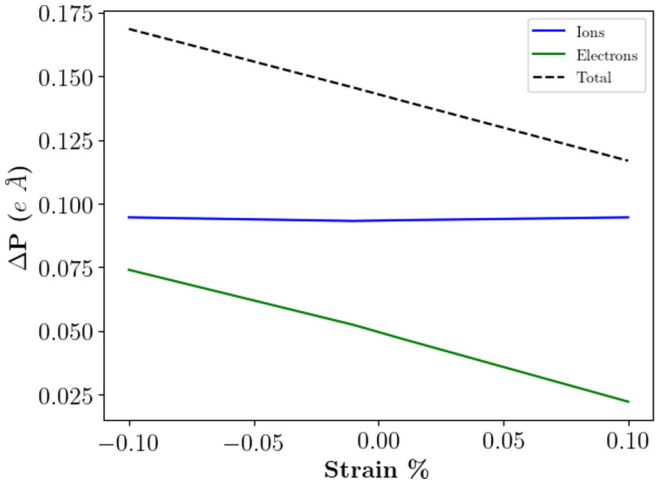

FIG. 7. Ionic and electronic contributions to the change in polarization of the DTN unit cell under applied strain.

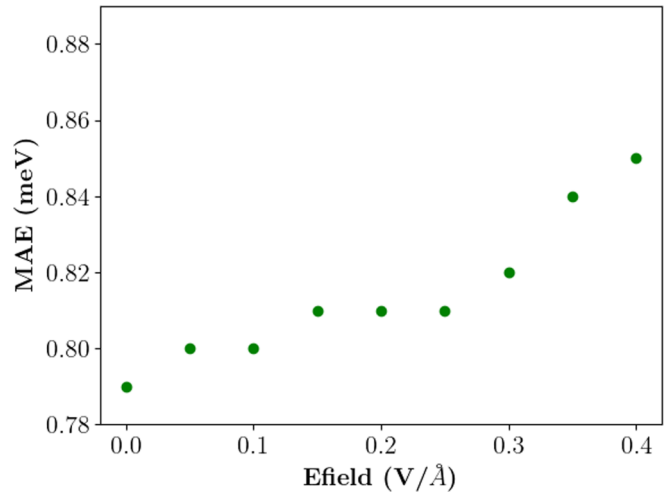

FIG. 8. The dependence of the magnetic anisotropy of bulk DTN on an electric field applied parallel to the *ab* plane.

spin-polarized state at high magnetic fields. Similarly, a 90° angle corresponds to spins lying on the *ab* plane and the *XY*-AFM state. For each configuration we calculated the electric dipole moment of the crystal within the modern theory of polarization framework [24]. What we see in Fig. 6 is that as the canting angle θ increases, and the spins approach the *ab* plane, there is a correlated decrease in the electric dipole moment (blue) of the crystal together with the expected decrease in M_z (red). This indicates the presence of a ME coupling within the DTN molecular crystal.

To probe the mechanism responsible for the ME coupling we investigate what effect straining the molecular crystal has on the electronic polarization. The literature suggests magnetic field-induced strain, i.e., magnetostriction, changes the unit cell and a reorientation of the electrically polar ligands may be responsible for the change in polarization [3]. To test this, we used the DTN molecular crystal and the GGA-D3 functional structures from our ME calculations with collinear spins in an AFM configuration and no spin-orbit interaction. We applied a tensile strain on the DTN unit cell along the *c* axis of up to 0.1% while correspondingly compressing the *a*, *b* lattice constants, keeping the volume constant, and allowed the ions to relax to minimize the total energy. Similarly, we applied a compression to the *c* lattice constant while expanding the *a*, *b* constants. We calculated the polarization as a function of applied strain. We distinguish the change in polarization relative to the unstrained system ΔP, resulting from ionic motion (blue) from that due to changes in electronic density (green) in Fig. 7. The results indicate that the main contribution to the change in polarization comes from subtle changes in electronic density rather than a reorientation of the thiourea ligands. An analysis of the molecular crystal structure shows little variation in the Cl-Ni-S bond angles or bond lengths, supporting this result.

To conclude our paper of the ME effect in DTN, we investigate what effect applying an electric field has on the magnetic properties of the molecular crystal. Specifically, we investigate the MAE) as a function of electric-field strength where the electric field is aligned parallel to the *a* axis and perpendicular to the 1D chain. In these calculations we used the DTN molecular crystal unit cell structure with two Ni atoms and the GGA-D3 + U exchange-correlation functional with $U_{\text{eff}} = 6$ eV. As with our previous MAE calculations, we performed noncollinear magnetic DFT calculations including spin-orbit interactions and obtained the energy difference between two configurations of spins aligned 90° relative to one another. The results show that by increasing the strength of the electric field, we are able to increase the MAE of bulk DTN (Fig. 8). This indicates the presence of a reverse coupling in this molecular crystal, not observed experimentally, showing that the magnetic properties may be tuned by electronic means.

IV. CONCLUSION

Our aim in this paper has been an attempt to model DTN within a DFT framework. This approach not only provides a way to gain insight into the mechanisms responsible for structural, electronic, and magnetic properties, but also allows us to make accurate predictions while minimizing the computational cost. We were able to show that the inclusion of the GGA-D3 correction substantially improves the structure of the DTN molecular crystal, providing accurate lattice constants, bond lengths, and bond angles. Adding the Hubbard term to the standard GGA functional allowed us to improve our modeling of the magnetic interactions in DTN, accurately predicting the magnetic anisotropy and exchange coupling constants and providing an additional J_{diag} coupling. The quasi-1D nature of DTN was indicated by the hybridization of Ni($d_{3z^2-r^2}$) and Cl-Cl antibonding orbitals via a virtual superexchange path along the *c* axis. Finally, we showed the presence of a ME coupling and predict an increase in magnetic anisotropy with the application of an electric field. The results of this paper are a first step towards understanding the detailed mechanisms involved in the magnetoelectric coupling in DTN. Its presence in functional organic quantum magnets

suggests the possibility of future applications where the magnetic properties of materials may be fine-tuned through more feasible structural and electronic means. Yet to be explored in detail is the nature of Bose-Einstein condensates in organic quantum magnets [7] and the important role the ME effect plays in this state. We hope this paper puts forward the idea that these fundamental properties may be investigated from first principles.

ACKNOWLEDGMENTS

This work was supported as part of the Center for Molecular Magnetic Quantum Materials, an Energy Frontier Research Center funded by the US Department of Energy, Office of Science, Basic Energy Sciences under Award No. DE-SC0019330. Computations were performed at NERSC and UFRC.

[1] S. Fusil, V. Garcia, A. Barthélémy, and M. Bibes, magnetoelectric devices for spintronics, Annu. Rev. Mater. Res. **44**, 91 (2014).

[2] V. Zapf, F. Wolff-Fabris, M. Kenzelmann, F. Nasreen, F. Balakirev, Y. Chen, and A. Paduan-Filho, Multiferroic behavior in organo-metallics, J. Phys.: Conf. Ser. **273**, 012132 (2011).

[3] V. S. Zapf, V. F. Correa, P. Sengupta, C. D. Batista, M. Tsukamoto, N. Kawashima, P. Egan, C. Pantea, A. Migliori, J. B. Betts, M. Jaime, and A. Paduan-Filho, Direct measurement of spin correlations using magnetostriction, Phys. Rev. B **77**, 020404(R) (2008).

[4] O. Sato, Dynamic molecular crystals with switchable physical properties, Nat. Chem. **8**, 644 (2016).

[5] A. Lopez-Castro and M. R. Truter, 245. the crystal and molecular structure of dichlorotetrakisthioureanickel, [(nh2)2cs]4nicl2, J. Chem. Soc. (Resumed), 1309 (1963).

[6] E. Mun, J. Wilcox, J. L. Manson, B. Scott, P. Tobash, and V. S. Zapf, The origin and coupling mechanism of the magnetoelectric effect in tmcl2-4sc(nh2)2 (tm = ni and co), Adv. Condens. Matter Phys. **2014**, 512621 (2014).

[7] R. Yu, L. Yin, N. S. Sullivan, J. Xia, C. Huan, A. Paduan-Filho, N. F. Oliveira Jr, S. Haas, A. Steppke, C. F. Miclea *et al.*, Bose glass and mott glass of quasiparticles in a doped quantum magnet, Nature (London) **489**, 379 (2012).

[8] A. Orlova, R. Blinder, E. Kermarrec, M. Dupont, N. Laflorencie, S. Capponi, H. Mayaffre, C. Berthier, A. Paduan-Filho, and M. Horvatić, Nuclear Magnetic Resonance Reveals Disordered Level-Crossing Physics in the Bose-Glass Regime of the Br-Doped $Ni(Cl_{1-x}Brx)_2 - 4SC(NH_2)_2$ Compound at a High Magnetic Field, Phys. Rev. Lett. **118**, 067203 (2017).

[9] M. Dupont, S. Capponi, M. Horvatić, and N. Laflorencie, Competing Bose-glass physics with disorder-induced Bose-Einstein condensation in the doped S=1 antiferromagnet $Ni(Cl_{1-x}Brx)_2 - 4SC(NH_2)_2$ at high magnetic fields, Phys. Rev. B **96**, 024442 (2017).

[10] A. Paduan-Filho, Bose-einstein condensation of magnons in $NiCl_{2-4}SC(NH_2)_2$, Braz. J. Phys. **42**, 292 (2012).

[11] P. Hohenberg and W. Kohn, Inhomogeneous electron gas, Phys. Rev. **136**, B864 (1964).

[12] W. Kohn and L. J. Sham, Self-consistent equations including exchange and correlation effects, Phys. Rev. **140**, A1133 (1965).

[13] G. Kresse and J. Furthmüller, Efficiency of *ab-initio* total energy calculations for metals and semiconductors using a plane-wave basis set, Comput. Mater. Sci. **6**, 15 (1996).

[14] G. Kresse and J. Furthmüller, Efficient iterative schemes forab initiototal-energy calculations using a plane-wave basis set, Phys. Rev. B **54**, 11169 (1996).

[15] P. E. Blöchl, Projector augmented-wave method, Phys. Rev. B **50**, 17953 (1994).

[16] G. Kresse and D. Joubert, From ultrasoft pseudopotentials to the projector augmented-wave method, Phys. Rev. B **59**, 1758 (1999).

[17] J. P. Perdew, K. Burke, and M. Ernzerhof, Generalized Gradient Approximation Made Simple, Phys. Rev. Lett. **77**, 3865 (1996).

[18] S. L. Dudarev, G. A. Botton, S. Y. Savrasov, C. J. Humphreys, and A. P. Sutton, Electron-energy-loss spectra and the structural stability of nickel oxide: An LSDA+U study, Phys. Rev. B **57**, 1505 (1998).

[19] S. Grimme, S. Ehrlich, and L. Goerigk, Effect of the damping function in dispersion corrected density functional theory, J. Comput. Chem. **32**, 1456 (2011).

[20] H. J. Monkhorst and J. D. Pack, Special points for brillouin-zone integrations, Phys. Rev. B **13**, 5188 (1976).

[21] N. Marzari and D. Vanderbilt, Maximally localized generalized wannier functions for composite energy bands, Phys. Rev. B **56**, 12847 (1997).

[22] A. A. Mostofi, J. R. Yates, Y.-S. Lee, I. Souza, D. Vanderbilt, and N. Marzari, wannier90: A tool for obtaining maximally-localised wannier functions, Comput. Phys. Commun. **178**, 685 (2008).

[23] I. Souza, N. Marzari, and D. Vanderbilt, Maximally localized wannier functions for entangled energy bands, Phys. Rev. B **65**, 035109 (2001).

[24] R. D. King-Smith and D. Vanderbilt, Theory of polarization of crystalline solids, Phys. Rev. B **47**, 1651(R) (1993).

[25] D. Vanderbilt and R. D. King-Smith, Electric polarization as a bulk quantity and its relation to surface-charge, Phys. Rev. B **48**, 4442 (1993).

[26] https://www.vasp.at/wiki/index.php/Berry_phases_and_finite_electric_fields.

[27] I. Souza, J. Iniguez, and D. Vanderbilt, First-Principles Approach to Insulators in Finite Electric Fields, Phys. Rev. Lett. **89**, 117602 (2002).

[28] R. W. Nunes and X. Gonze, Berry-phase treatment of the homogeneous electric field perturbation in insulators, Phys. Rev. B **63**, 155107 (2001).

[29] H.-P. Cheng, S. Liu, X. Chen, L. Zhang, and J. N. Fry, First-principles study of magnetism and electric field effects in 2d systems, AVS Quantum Sci. **2**, 027101 (2020).

[30] L. Kronik and A. Tkatchenko, Understanding molecular crystals with dispersion-inclusive density functional theory: Pairwise corrections and beyond, Acc. Chem. Res. **47**, 3208 (2014).

[31] J. Klimeš, D. R. Bowler, and A. Michaelides, Chemical accuracy for the van der waals density functional, J. Phys.: Condens. Matter **22**, 022201 (2009).

[32] K. Lee, É. D. Murray, L. Kong, B. I. Lundqvist, and D. C. Langreth, Higher-accuracy van der waals density functional, Phys. Rev. B **82**, 081101(R) (2010).

[33] F. Aryasetiawan, M. Imada, A. Georges, G. Kotliar, S. Biermann, and A. I. Lichtenstein, Frequency-dependent local interactions and low-energy effective models from electronic structure calculations, Phys. Rev. B **70**, 195104 (2004).

[34] F. Aryasetiawan, K. Karlsson, O. Jepsen, and U. Schönberger, Calculations of Hubbard U from first-principles, Phys. Rev. B **74**, 125106 (2006).

[35] A. Kozhevnikov, A. G. Eguiluz, and T. C. Schulthess, Toward first principles electronic structure simulations of excited states and strong correlations in nano- and materials science, in *2010 ACM/IEEE International Conference for High Performance Computing, Networking, Storage and Analysis, Denver, CO, 2010* (IEEE, Piscataway, NJ, 2010).

[36] L. Zhang, P. Staar, A. Kozhevnikov, Y.-P. Wang, J. Trinastic, T. Schulthess, and H.-P. Cheng, DFT + DMFT calculations of the complex band and tunneling behavior for the transition metal monoxides MnO, FeO, CoO, and NiO, Phys. Rev. B **100**, 035104 (2019).

[37] J. P. Allen and G. W. Watson, Occupation matrix control of *d*- and *f*-electron localisations using DFT + U, Phys. Chem. Chem. Phys. **16**, 21016 (2014).

[38] T. Cai, H. Han, Y. Yu, T. Gao, J. Du, and L. Hao, Study on the ground state of NiO: The LSDA (GGA)+ U method, Physica B **404**, 89 (2009).

[39] E. R. Ylvisaker, W. E. Pickett, and K. Koepernik, Anisotropy and magnetism in the LSDA + U method, Phys. Rev. B **79**, 035103 (2009).

[40] See Supplemental Material at http://link.aps.org/supplemental/10.1103/PhysRevB.103.054434 for the details of an alternative WF-based Hamiltonian near the Fermi level.

[41] A. E. Thuijs, X.-G. Li, Y.-P. Wang, K. A. Abboud, X.-G. Zhang, H.-P. Cheng, and G. Christou, Molecular analogue of the perovskite repeating unit and evidence for direct Mn^{III}-Ce^{IV}-Mn^{III} exchange coupling pathway, Nat. Commun. **8**, 500 (2017).

[42] F. Zhou and V. Ozolins, Obtaining correct orbital ground states in *f*-electron systems using a nonspherical self-interaction-corrected LDA + U method, Phys. Rev. B **80**, 125127 (2009).

[43] J. Gu, S. Liu, M. Yazback, H.-P. Cheng, and X.-G. Zhang, Many-body localization from random magnetic anisotropy, Phys. Rev. Research **1**, 033183 (2019).